

System identification of highway bridges from ambient vibration using subspace stochastic realization theories

Md. Rajab Ali*¹ and Takatoshi Okabayashi²

¹*Graduate School of Science and Technology, Nagasaki University
1-14, Bunkyo machi, Nagasaki 852-8521, Japan*

²*Department of Civil Engineering, Faculty of Engineering, Nagasaki University
1-14, Bunkyo machi, Nagasaki 852-8521, Japan*

(Received September 2, 2010 , Accepted December 14, 2010)

Abstract. In this study, the subspace stochastic realization theories (SSR model I and SSR model II) have been applied to a real bridge for estimating its dynamic characteristics (natural frequencies, damping constants, and vibration modes) under ambient vibration. A numerical simulation is carried out for an arch-type steel truss bridge using a white noise excitation. The estimates obtained from this simulation are compared with those obtained from the Finite Element (FE) analysis, demonstrating good agreement and clarifying the excellent performance of this method in estimating the structural dynamic characteristics. Subsequently, these methods are applied to the vibration induced by both strong and weak winds as obtained by remote monitoring of the Kabashima bridge (an arch-type steel truss bridge of length 136 m, and situated in Nagasaki city). The results obtained with this experimental data reveal that more accurate estimates are obtained when strong wind vibration data is used. In contrast, the vibration data obtained from weak wind provides accurate estimates at lower frequencies, and inaccurate accuracy for higher modes of vibration that do not get excited by the wind of lower intensity. On the basis of the identified results obtained using both simulated data and monitored data from a real bridge, it is determined that the SSR model II realizes more accurate results than the SSR model I. In general, the approach investigated in this study is found to provide acceptable estimates of the dynamic characteristics of highway bridges as well as for the vibration monitoring of bridges.

Keywords: structural health monitoring; system identification; ambient vibration; bridge dynamic characteristics; subspace stochastic realization theory.

1. Introduction

During past few decades, many bridges were constructed even in remote areas especially in developed countries. These structures are now starting to age rather rapidly. Consequently, a low-cost maintenance and management system is required to maintain them in a safe and effective functioning state (Shohn *et al.* 2003, Takewaki and Nakamura 2005) and new methods have been developed recently (Moustafa *et al.* 2010).

The recent advances in communications technology and in personal computers in conjunction with improved measurement technology have made it more realistic to contemplate monitoring the

* Corresponding author, Ph.D., E-mail: rajab_ali@stu.civil.nagasaki-u.ac.jp

dynamic behavior of highway bridges in remote areas. Furthermore, highly accurate estimates of highway bridge dynamic characteristics (natural frequencies, damping constants, and vibration modes) are now possible through the application of realization theories to highway bridge under wind and moving vehicle loadings. There is now an urgent need to bring these together in a technology for investigating bridge deterioration and damage based on monitored vibration information.

A useful method of identifying damage and deterioration in highway bridges, which gives highly accurate results, is to automatically estimate the structural dynamic characteristics under ambient vibration. The modal analysis method has been proposed for estimating the structural dynamic behavior from measured vibration data (Jimin and Zhi-Fang 2001). Meanwhile, realization theories have been proposed as part of the control theory, giving rise to major advances in research on estimating the bridge dynamic characteristics (Jaung 1994, Jaung *et al.* 1985, Gevers *et al.* 2006). In this approach, the dynamic properties are estimated from the transfer function or the impulse response function obtained using input-output data for the structure.

For large-scale civil structures, such as, long-span highway bridges, it is difficult to implement the vibration tests using artificial forces. In contrast, the large surface area of a bridge makes it susceptible to wind interactions leading to long-time vibrations. These vibrations are assumed to be similar to the stationary response of a structure under white noise excitation, and, are modeled as stochastic processes. When this approach of characterization is adopted, only the output data is required to estimate the structural dynamic characteristics. The stochastic realization theory (Nagayama *et al.* 2005, Sirinngoringo and Fujino 2008) and also the multi-dimensional ARMA model (Garibaldi *et al.* 1998, Papakos and Fassios 2003, Carden and Brownjohn 2008) for modal parameters estimation are useful to separate significant information about structural dynamic characteristics from the stationary stochastic process.

Akaike (1976) proposed a method for estimating the state space model from the canonical correlation of a stochastic process. In a later study, Desai *et al.* (1985) proposed further improvements to this theory in an enhancement known as subspace stochastic realization. Successive extension of this theory has been introduced based on the techniques used for estimating the system matrices. Aoki (1987) estimated the system matrices using canonical correlations between the future and past observations, where it is possible to estimate system matrices A and C from an identifiable state vector (Overschee and Moor 1996). The approaches correspond to the SSR model I and SSR model II, respectively. These methods provide protection against noisy data since they adopt several robust numerical techniques, such as, the LQ decomposition, the SVD, and the least-squares method (Overschee and Moor 1996, Abdelghani *et al.* 1998, Katayama 2005). Due to their remarkable advantages, these theories have been effectively applied to simulated and real structural data (Baseville *et al.* 2001, Peeters and Roeck 2001, Reynders and Roeck 2008). However, a few studies have considered the influence of the ambient vibration behavior, particularly, for the wind velocity on the estimation accuracy. This aspect still remains as a significant challenge to researchers.

To investigate the effectiveness of the subspace stochastic realization theories for automatic and remote structural vibration monitoring, numerical simulations for steel arch-bridges have been carried out. In the numerical example, the estimated results will be compared with those obtained using the FE analysis. The method is then used to investigate the ambient vibrations induced by strong and weak wind as obtained by the remote monitoring of Kabashima bridge (an arch-type steel truss bridge of length 136.0 m that is situated in Nagasaki city). The validity of this method for the monitoring of real bridge vibrations is also investigated.

2. Structure modeling

The dynamic behavior of a highway bridge is modeled using the finite element method. It is expressed by an n -dof system equation of motion

$$\mathbf{m}\ddot{\mathbf{z}}(t) + \mathbf{c}\dot{\mathbf{z}}(t) + \mathbf{kz}(t) = \mathbf{d}\mathbf{w}(t) \quad (1)$$

where $\mathbf{z}(t) \in \mathbf{R}^n$ is the displacement vector at continuous time t and $\mathbf{w}(t) \in \mathbf{R}^l$ is the external force. Terms $\mathbf{m} \in \mathbf{R}^{n \times n}$, $\mathbf{c} \in \mathbf{R}^{n \times n}$, $\mathbf{k} \in \mathbf{R}^{n \times n}$ and $\mathbf{d} \in \mathbf{R}^{n \times l}$ are the mass, general viscous damping, stiffness matrix, and external force acting on the l th node of the bridge.

For stochastic realization, Eq. (1) needs to be rearranged in its discrete form (Reyenders and Roeck 2008). Let the equally spaced continuous times t be given by $0, T, 2T, \dots, kT, \dots$ where T is constant time interval. Considering initial time $t_k = kT$, and the time after T interval, i.e. $t_{k+1} = (k+1)T$, we can get the discrete time state space equations as shown in equations below

$$\mathbf{x}(k+1) = \mathbf{A}\mathbf{x}(k) + \mathbf{B}\mathbf{w}(k) \quad (2a)$$

$$\mathbf{y}(k) = \mathbf{C}\mathbf{x}(k) + \mathbf{D}\mathbf{w}(k) \quad (2b)$$

where $\mathbf{y}(k) \in \mathbf{R}^m$ is the m -point observation data, k is discrete time and $k \geq 0$. $\mathbf{A} \in \mathbf{R}^{2n \times 2n}$ is the state matrix, characterizing the system dynamic properties and $\mathbf{B} \in \mathbf{R}^{2n \times l}$ is the external force matrix. $\mathbf{w}(k) \in \mathbf{R}^l$ is an unmeasurable vector signal, taken as a zero mean white noise, $\mathbf{C} \in \mathbf{R}^{m \times 2n}$ is the observation matrix, and $\mathbf{D} \in \mathbf{R}^{m \times l}$ is the direct transmission matrix.

3. Subspace stochastic realization theories

3.1 Basic formulation

Consider $\{\mathbf{y}(t), t = 1, 2, \dots, N + 2k - 2\}$ as the measured data over finite time for sufficiently large values of N with $k > 0$ and $\mathbf{y}(k)$ as the measurement data for present time t . In this condition, the past and future response data blocks $\mathbf{Y}_p \in \mathbf{R}^{m \times k \times N}$ and $\mathbf{Y}_f \in \mathbf{R}^{m \times k \times N}$ have the definitions

$$\mathbf{Y}_p = \begin{bmatrix} \mathbf{y}(k-1) & \dots & \mathbf{y}(N+k-2) \\ \mathbf{y}(k-2) & \dots & \mathbf{y}(N+k-3) \\ \vdots & & \vdots \\ \mathbf{y}(0) & \dots & \mathbf{y}(N-1) \end{bmatrix} \quad (3)$$

$$\mathbf{Y}_f = \begin{bmatrix} \mathbf{y}(k) & \mathbf{y}(k+1) & \dots & \mathbf{y}(N+k-1) \\ \mathbf{y}(k+1) & & \dots & \mathbf{y}(N+k) \\ \vdots & & & \vdots \\ \mathbf{y}(2k-1) & \dots & \dots & \mathbf{y}(N+2k-2) \end{bmatrix} \quad (4)$$

Throughout this paper the superscript T represents the transpose operator. Using Eqs. (3) and (4), the auto covariance and orthogonal covariance of \mathbf{Y}_p and \mathbf{Y}_f are obtained, as follows

$$\begin{bmatrix} \Lambda_{pp} & \Lambda_{pf} \\ \Lambda_{fp} & \Lambda_{ff} \end{bmatrix} = \frac{1}{N} \begin{bmatrix} \mathbf{Y}_p \\ \mathbf{Y}_f \end{bmatrix} \begin{bmatrix} \mathbf{Y}_p^T & \mathbf{Y}_f^T \end{bmatrix} \quad (5)$$

It should be noted that the cross covariance sequences $\frac{1}{N}[\mathbf{Y}_f \mathbf{Y}_p^T]$ satisfy the definition of Hankel matrix \mathbf{H} whereas; the auto covariance sequences $\frac{1}{N}[\mathbf{Y}_f \mathbf{Y}_f^T]$ and $\frac{1}{N}[\mathbf{Y}_p \mathbf{Y}_p^T]$ are the Toeplitz matrices \mathbf{T}_+ and \mathbf{T}_- respectively. Now allowing the LQ decomposition such that

$$\frac{1}{\sqrt{N}} \begin{bmatrix} \mathbf{Y}_p \\ \mathbf{Y}_f \end{bmatrix} = \begin{bmatrix} \mathbf{L}_{11} & 0 \\ \mathbf{L}_{21} & \mathbf{L}_{22} \end{bmatrix} \begin{bmatrix} \mathbf{Q}_1^T \\ \mathbf{Q}_2^T \end{bmatrix} \quad (6)$$

Accordingly, the covariance of the measurement data is calculated by

$$\begin{bmatrix} \Lambda_{pp} & \Lambda_{pf} \\ \Lambda_{fp} & \Lambda_{ff} \end{bmatrix} = \begin{bmatrix} \mathbf{L}_{11} & 0 \\ \mathbf{L}_{21} & \mathbf{L}_{22} \end{bmatrix} \begin{bmatrix} \mathbf{L}_{11}^T & \mathbf{L}_{21}^T \\ 0 & \mathbf{L}_{22}^T \end{bmatrix} \quad (7)$$

where $\Lambda_{fp} = \mathbf{L}_{21} \mathbf{L}_{11}^T$, $\Lambda_{pp} = \mathbf{L}_{11} \mathbf{L}_{11}^T$ and $\Lambda_{ff} = \mathbf{L}_{21} \mathbf{L}_{21}^T + \mathbf{L}_{22} \mathbf{L}_{22}^T$, are finite dimensional approximations over the infinite dimensional Hankel matrix \mathbf{H} and Toeplitz matrices \mathbf{T}_+ , \mathbf{T}_- respectively (e.g. Katayama 2005). Based on Eq. (7), two methods of subspace stochastic realization are proposed (e.g. Aoki 1987, Overschee and Moor 1996) and these methods are summarized below.

3.1.1 Subspace stochastic realization (SSR model I)

Using full rank factorization, square root matrices of the covariance matrices $\Lambda_{ff} = \mathbf{L} \mathbf{L}^T$ and $\Lambda_{pp} = \mathbf{M} \mathbf{M}^T$ are estimated. The SVD of the normalized covariance matrix $\mathbf{L}^{-1} \Lambda_{ff} \mathbf{M}^{-T} = \mathbf{U} \mathbf{S} \mathbf{V}^T = \mathbf{U}_n \mathbf{S}_n \mathbf{V}_n^T$. Notably, the SVD is executed so as to satisfy the conditions $\mathbf{S}_n = \text{diag}(\sigma_1, \sigma_2, \sigma_3 \dots \sigma_n)$, $1 \geq \sigma_1 \geq \sigma_2 \dots \geq \sigma_n > 0$ and $\mathbf{U}_n^T \mathbf{U}_n = \mathbf{I}_n$, $\mathbf{V}_n^T \mathbf{V}_n = \mathbf{I}_n$. The extended observability matrix is given as $\mathbf{P}_k = \mathbf{L} \mathbf{U}_n \mathbf{S}_n^{\frac{1}{2}}$. Finally, the matrices \mathbf{A} , \mathbf{C} are given as

$$\mathbf{A} = \underline{\mathbf{P}}_k^+ \bar{\mathbf{P}}_k, \quad \mathbf{C} = \mathbf{P}_k(1:m,:), \quad (8)$$

where, $\underline{\mathbf{P}}_k = \mathbf{P}_k(km - m, :)$ and $\bar{\mathbf{P}}_k = \mathbf{P}_k(m + 1:km, :)$ are the matrices formed by excluding the lower and upper m rows of \mathbf{P}_k .

3.1.2 Subspace stochastic realization (SSR model II)

The n -dimensional state vector can be expressed as follows

$$\bar{\mathbf{X}}_k = \mathbf{S}_n^{\frac{1}{2}} \mathbf{V}_n^T \mathbf{M}^{-1} \mathbf{Y}_p \quad \text{and} \quad \mathbf{Y}_{k/k} = [\mathbf{y}(k) \cdots \cdots \mathbf{y}(k+N-1)] \quad (9)$$

Now, the projected vectors $\hat{\mathbf{X}}_{k+1}$ and $\hat{\mathbf{Y}}_{k/k}$ that are calculated by retaining to column $N-1$ of $\bar{\mathbf{X}}_k$ and $\mathbf{Y}_{k/k}$ yield the following equation

$$\begin{bmatrix} \hat{\mathbf{X}}_{k+1} \\ \hat{\mathbf{Y}}_{k/k} \end{bmatrix} = \begin{bmatrix} \mathbf{A} \\ \mathbf{C} \end{bmatrix} \hat{\mathbf{X}}_k + \begin{bmatrix} \boldsymbol{\rho}_w \\ \boldsymbol{\rho}_v \end{bmatrix} \quad ((n+m) \times ((N-1))) \quad (10)$$

where, $\boldsymbol{\rho}_w \in \mathbf{R}^s$ and $\boldsymbol{\rho}_v \in \mathbf{R}^m$ are the estimation errors to be considered as white noise. Thus, the coefficient matrices A and C can be estimated from Eq. (10) using the least squares method.

3.2 Dynamic characteristics estimation

The well-known relationships between the eigenvalues of continuous (λ_k, λ_k^*) and discrete (μ_k, μ_k^*) time system matrices are $\mu_k = e^{\lambda_k T}$ and $\mu_k^* = e^{\lambda_k^* T}$, which give the following relations

$$\omega_{dk} = \frac{1}{T} \tan^{-1} \left| \frac{\mu_k - \mu_k^*}{\mu_k + \mu_k^*} \right|, \quad \sigma_k = -\frac{1}{2T} \ln(\mu_k \mu_k^*) \quad (11)$$

where T is the data sampling time and $\omega_{dk} = \omega_k \sqrt{1 - h_k^2}$ is the damped natural frequency. By simple mathematical manipulation of Eq. (11), the eigen frequencies ω_k and damping constants h_k are estimated by

$$\omega_k = \sqrt{\omega_{dk}^2 + \sigma_k^2}, \quad h_k = \sigma_k / \omega_k \quad (12)$$

The vibration mode $\hat{\boldsymbol{\Phi}} \in \mathbf{C}^{m \times 2n}$ is found as

$$\hat{\boldsymbol{\Phi}} = \mathbf{C} \boldsymbol{\Phi} \quad (13)$$

where $\boldsymbol{\Phi} \in \mathbf{C}^{2n \times 2n}$ is the eigenvector matrix.

3.3 Dynamic characteristics extraction process

The selection of non-zero singular values facilitates finding the true model order, but in case of ambient vibration or noisy vibration signal, it is difficult to distinguish the zero and the non-zero singular values. Consequently, we have to consider over rank model, resulted in the estimation of noise corrupted system matrix. This noise is significantly influencing the higher mode dynamic parameters and the estimation accuracy. To overcome this problem, a new guide line are hereby proposed by the authors .

The eigenvalues of the discrete time system matrix A as derived in Eqs.(8) and (10) can be expressed by the following equation

$$\mu_k = e^{-h_k \omega_k T} (\cos \omega_{dk} T + i \sin \omega_{dk} T) \quad (14)$$

These eigenvalues are expressed in the polar coordinate system on a complex plane. In Fig. 1, the variable radius r , and the angle θ correspond to the real and the imaginary parts of the eigenvalues, respectively. This leads to the following relations

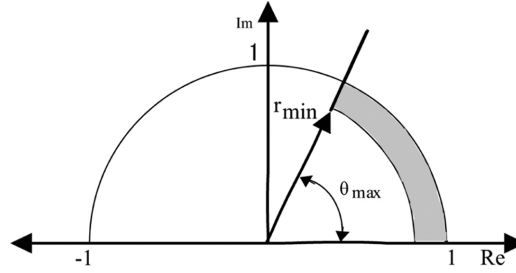


Fig. 1 Eigenvalues in polar coordinates, Eigenvalues exist in the shaded area are extracted for systems true eigenvalues

$$r = e^{-h_k \omega_k T}, \quad \theta = \tan^{-1} \omega_{dk} T \cong \tan^{-1} \omega_k T \quad (15)$$

Then, the general boundary conditions are established such that

$$r_{\min} < r < 1, \quad 0 < \theta < \theta_{\max} \quad (16)$$

where, $r_{\min} = e^{-h_{\max} \omega_{\max} T}$ and $\theta_{\max} = \tan^{-1} \omega_{\max} T$. Note that $\omega_{\max} = \pi/T$ and h_{\max} are the maximum natural frequencies and the maximum damping constants, respectively. Hence, the eigenvalues that fall within r_{\min} , θ_{\max} , are considered as the system's eigenvalues. Notably, the maximum damping constants should not be smaller than the standard values for the material used in structural system.

The vibration modes are estimated from the respective eigenvectors using the following equation

$$\hat{\Phi} = \begin{bmatrix} \phi_{11} & \cdots & \phi_{1p} \\ \vdots & \ddots & \vdots \\ \phi_{m1} & \cdots & \phi_{mp} \end{bmatrix} \quad (17)$$

where, p is the number of frequencies to be estimated. Corresponding to each eigenvalue μ_k , there exists a eigenvector ϕ_k and thus eigenvectors are given by the k th vector of the identified eigenvector matrix as follows.

$$\hat{\Phi}_k = \begin{bmatrix} \phi_{1k} \\ \phi_{mk} \end{bmatrix} \quad (18)$$

3.4 Parameter estimation

As noted in relation to Eq. (3), the size of N and k has a significant effect on estimation accuracy. If the values of N and k are too small, poor accuracy results, whereas selection of large values increases the size of the Hankel and Toeplitz matrices leading to significantly higher computational load. Consequently, it is crucial that the Hankel and Toeplitz matrices are of the optimum size. Besides, the length of the singular values n introduced in section 3.1.1 has to be considered carefully. From the physical appearance of singular values, it is clear that zero or near zero singular values should be discarded. We then optimized the size of H and T and the singular values for use in the estimation process. This optimization may not ensure the true model order because the exact information of the dynamic characteristics is not pre-determined. Therefore, we need further

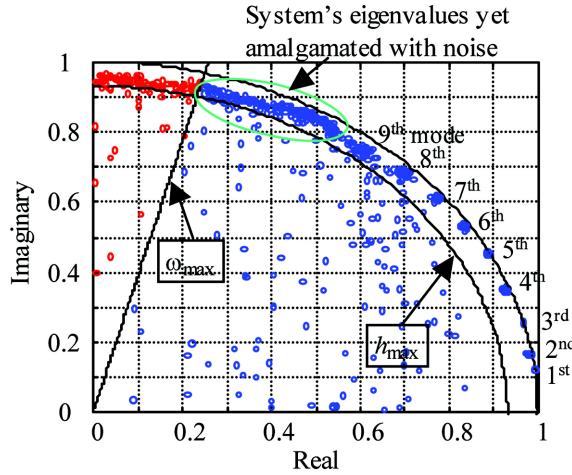


Fig. 2 Eigenvalues plotted on a complex plane, 1 st-9 th mode are the systems real eigenvalues considered for estimation; The eigenvalues existing inconsistently have to be neglected as the spurious mode or noise

filtration of the eigenvalues to separate the systems real mode. To illustrate this procedure, Fig. 2 has been drawn showing how the systems eigenvalues are collected from the specified area. In this figure, the eigenvalues are gathered at a specific point considered as the real mode, contrastingly, the noise or the spurious mode are plotted in a scattered way should be discarded. In this regard, the estimation accuracy is highly sensitive to the model parameters and the optimum values have to be found from the graphical presentation based on experience.

4. Ambient vibration simulation

4.1 General overview

In this section, a numerical simulation of a steel-truss highway bridge was carried out. The bridge was modeled by FE method and its natural frequencies, and vibration modes were calculated using eigenvalue analysis. Further we performed dynamic response analysis for white noise excitation. The calculated ambient vibration is then analyzed using the subspace stochastic realization theory to estimate the dynamic characteristics. We compared the results from eigenvalue analysis and SSR method to evaluate the estimation accuracy.

4.2 FE modeling of bridge and ambient vibration response estimation

For this numerical example, a steel truss bridge was selected as the model. The FEM bridge model consisted of 27 nodes, as shown in Fig. 3. The bridge and material specifications are given in Table 1. The eigen frequencies and vibration modes were calculated by eigenvalue analysis and are presented in Table 2 and Fig. 4, respectively. For dynamic analysis, white noise excitation was assumed to occur at all nodes. Outputs were collected in the vertical direction at nodes [2, 3, 4, 5, 6, 7, 8, 9, 10, 11, 12, 13]. Note that in carrying out response analysis, mass proportional damping

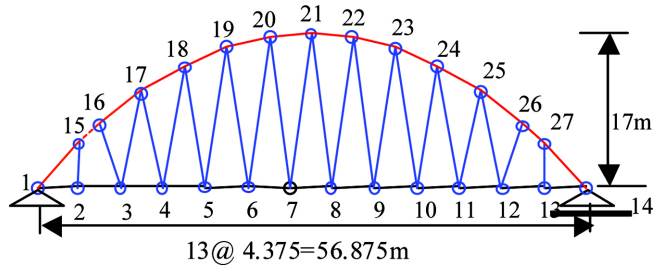


Fig. 3 FE model for the bridge; the numbers 1~27 indicate the node points

Table 1 Material specification for the FE model

Parameters	Valus
Effective span	56.88 m
Ridge	17.00 m
Density of steel	7850.00 Kg/m ³
Young's modulus	2.1×10 ¹¹ N/m ²

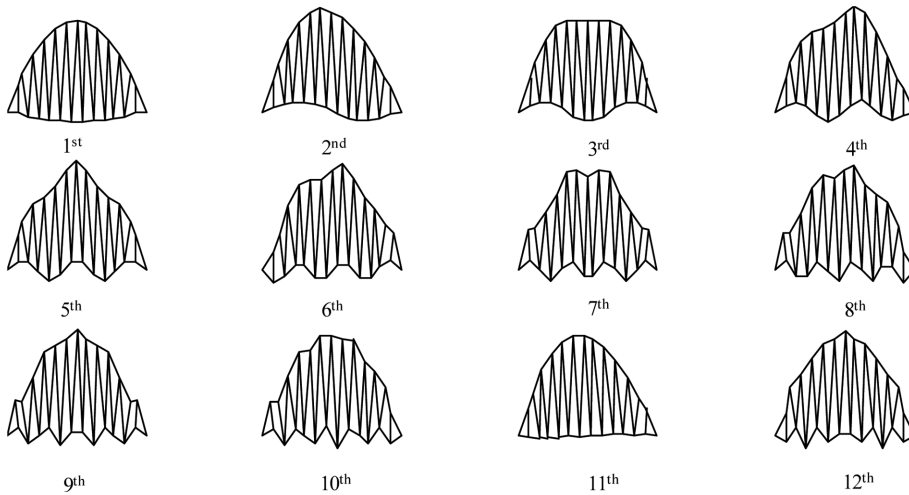


Fig. 4 Natural vibration modes calculated by eigenvalue analysis for the FE bridge model

($C = 2 * h_k * \omega_k * M$, numerical value of $h_k = 0.02$) is considered. The output velocity responses from 12 nodes were collected at the rate of 100 samples per second and analyzed using the subspace stochastic realization theories to calculate the dynamic characteristics (natural frequencies, damping constants, and vibration modes).

4.3 Dynamic characteristics estimation

As described above, response data obtained from the numerical simulation were used to estimate the dynamic characteristics. We divided one hundred fifty thousand (150,000) data points into fifty set and each set of data points (3000) were used to estimate dynamic characteristics (natural frequencies, damping constants, and vibration modes) for each times.

Table 2 Accuracy evaluation by comparing the natural frequencies and the damping constants estimated by the SSR methods with their analytical values and also observing the coefficient of variations (FE bridge model vibration data)

		Natural frequency(Hz)					Damping constant				
		Analytical mean	Estimated mean	Estimation errors(%)	Standard deviation.	Coefficient of Variations (%)	Assumed	Estimated mean	Estimation error (%)	Standard deviation	Coefficient of variation (%)
1 st	SSR model I	1.938	1.935	0.18	0.0196	1.01	0.02	0.023	15.00	0.0111	48.44
	SSR model II		1.963	1.30	0.0161	0.82		0.0086	57.00	0.0037	43.69
2 nd	SSR model I	2.619	2.620	0.03	0.0166	0.63	0.02	0.0185	7.50	0.0067	36.28
	SSR model II		2.680	2.34	0.0389	1.45		0.0222	11.00	0.0146	65.80
3 rd	SSR model I	4.141	4.107	0.81	0.0299	0.73	0.02	0.0165	17.50	0.0066	39.94
	SSR model II		4.133	0.20	0.0210	0.51		0.0048	76.00	0.0021	43.48
4 th	SSR model I	5.796	5.670	2.17	0.2376	4.19	0.02	0.0202	1.00	0.0151	74.72
	SSR model II		5.758	0.66	0.0535	0.93		0.022	10.00	0.0086	39.08
5 th	SSR model I	7.641	7.319	4.22	0.5237	7.16	0.02	0.0219	9.50	0.0103	47.16
	SSR model II		7.505	0.14	0.0427	0.57		0.0079	60.50	0.0031	38.81
6 th	SSR model I	9.353	8.881	5.05	0.5480	6.17	0.02	0.0213	6.50	0.0074	34.76
	SSR model II		9.089	2.82	0.0662	0.73		0.0209	4.50	0.0063	30.00
7 th	SSR model I	11.073	10.346	6.57	0.6786	6.56	0.02	0.0246	23.00	0.0084	34.28
	SSR model II		10.661	3.72	0.0594	0.56		0.0204	2.00	0.0131	64.51
8 th	SSR model I	12.957	11.919	8.01	0.7539	6.33	0.02	0.0253	26.50	0.0064	25.37
	SSR model II		12.310	5.00	0.2790	2.27		0.0325	62.50	0.0131	40.19
9 th	SSR model I	15.226	13.728	9.84	0.9094	6.62	0.02	0.023	15.00	0.0052	22.45
	SSR model II		14.123	7.24	0.5108	3.62		0.0449	124.50	0.0108	24.09
10 th	SSR model I	17.472	15.472	11.45	1.0306	6.66	0.02	0.0218	9.00	0.0047	21.71
	SSR model II		15.806	9.53	0.4042	2.56		0.0293	46.50	0.0080	27.46
11 th	SSR model I	18.662	16.603	11.03	0.8356	5.03	0.02	0.0169	15.50	0.0049	29.16
	SSR model II		16.798	9.99	0.3015	1.79		0.0221	10.50	0.0070	31.72
12 th	SSR model I	19.837	17.548	11.54	0.7147	4.07	0.02	0.0161	19.50	0.0048	30.04
	SSR model II		17.916	9.68	0.6822	3.81		0.0326	63.00	0.0098	30.18

System identification of highway bridges from ambient vibration using subspace...

4.3.1 Natural frequencies

Estimated modal frequencies obtained from ambient vibration data using the SSR model II are shown in Fig. 5(a). From the first mode through the ninth mode, the estimation performance is excellent. On the other hand, estimated frequencies above the ninth mode appear more scattered. Table 2 compares the analytical values obtained with FEM with the theoretical results; estimated mean values, estimation errors, standard deviations, and coefficient of variations are listed for comparison. Estimation error was calculated such that

$$\text{Estimation error} = (\text{analytical value} - \text{estimated mean}) / \text{analytical value}$$

It is clear that there is an increasing tendency for estimation error as the mode increases. It can also be seen that the estimation errors are less for the SSR model II than for the SSR model I.

4.3.2 Damping constants

Damping constants were estimated by the SSR model I and SSR model II. The results obtained using the SSR model II are shown in Fig. 5(b). It is clear that estimated damping constants are more scattered than the estimated frequencies. The estimation accuracy for damping constants is compared in Table 2, demonstrating that the coefficient of variations generally remain within 74%. In general, the small values of the damping constants lead to some unpredictable computation

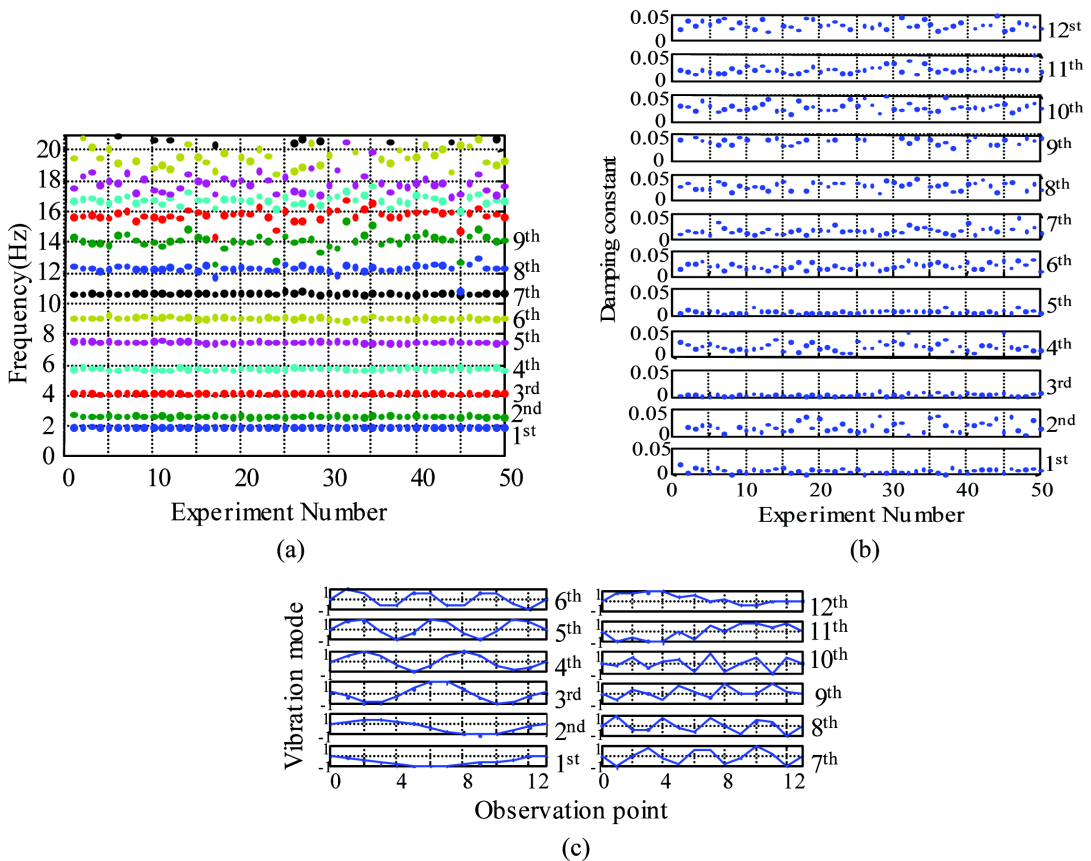


Fig. 5 Estimated dynamic characteristics (SSR model II): (a) Natural frequencies (Hz), (b) Damping constants, (c) Vibration modes

errors. The short length of record data produces errors on damping estimates but the frequency estimation still remains good. However, the obtained results for damping constants in this case can be claimed as good accuracy because the values of damping constants are numerically very small.

4.3.3 Vibration modes

Each vibration mode estimated by the SSR model II is graphically represented in Fig. 5(c). This figure is plotted using the average of fifty(50) repeated estimates. Similar vibration mode shapes are obtained also using the SSR model I. The results coincide well with those plotted from the FE analysis. This is a clear indication that reliable estimates of vibration modes are obtained using both methods up to the twelfth mode.

5. Automatic remote monitoring of ambient vibration

5.1 System preparation

The structure selected for remote monitoring of ambient vibration was the Kabashima highway bridge, built in 1986 and located in Nagasaki city. It is a steel girder bridge with a maximum span of 153 m, a total length of 227 m, and a width of 7.5 m. Fig. 6(a) shows a general view of the bridge and its location with respect to Nagasaki University. Instrumentation on the object bridge consisted of five sensors affixed along the bridge axis at equal intervals, with one sensor at bridge midpoint. The instrumentation system was housed in a box placed on the under-girder inspection walkway. The client PC was housed in a faculty of engineering research laboratory at Nagasaki University. Data were recorded at the rate of 100 samples per second at the sensors location, saved

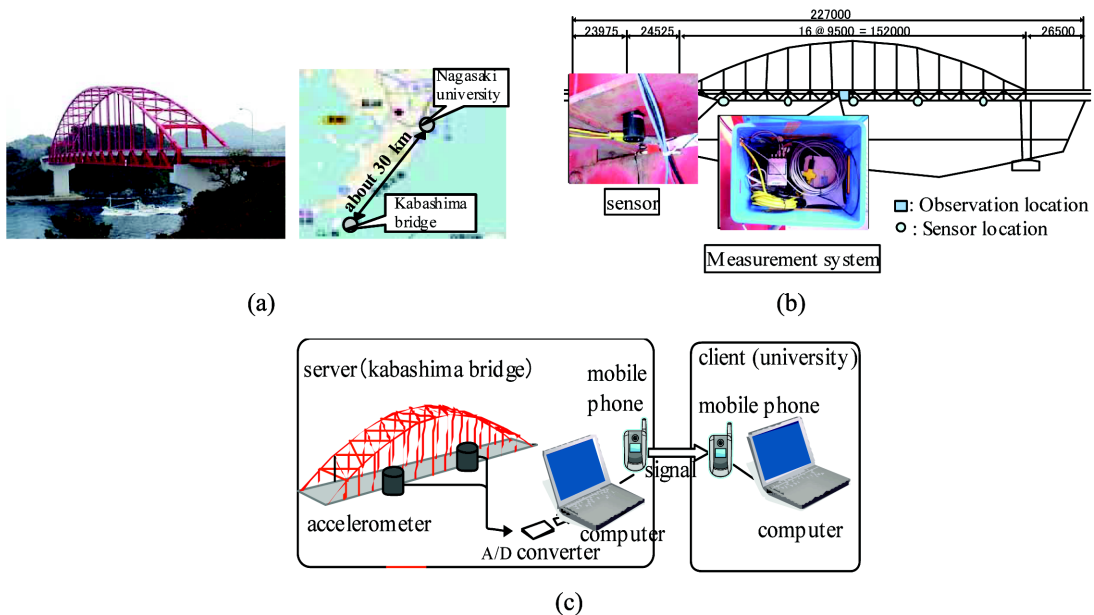


Fig. 6 Remote monitoring system: (a) General view and location of Kabashima bridge, (b) Equipment setup for instrumentation system, (c) Flow diagram of measurement system

in the server PC and every five minute's measurement data transmitted altogether to the client PC at regular interval. Figs. 6(b) and 6(c) show the arrangement and flow diagram of the measurement system. Dynamic characteristics (natural frequencies, damping constants, and vibration modes) were estimated from the automatically collected ambient vibration data by offline processing.

5.2 Measured ambient vibration data

As already described, ambient vibrations were recording by the remote instrumentation system. The bridge is located at the top end of the Nagasaki peninsula and faces continuous severe wind excitation. Especially, the summer storm is frequently passing across the bridge axis. Two main options were considered for sampling measurement data from the collected data set. The first was to choose vibrations induced by strong winds (speed = 8–11 m/s) collected during the summer storm, whereas the second option was to select data for weak winds (speed 1–3 m/s) measured under the normal wind conditions. In this report, these two samples are referred to as strong wind and weak wind data, respectively. To illustrate the general behavior of the measurement data, the power spectrum density (PSD) function has been calculated that are graphically presented in Figs. 7 and 8. Figs. 7(a) and 7(b) show the strong wind response and related power spectrum density, respectively. These figures show that during ambient vibration monitoring the bridge vibrated at high amplitude with uniform intensity. The data presented in Fig. 8(a) is the response measured under weak wind excitation, while Fig. 8(b) shows the related power spectrum density. These PSD plots also show clear peak in the lower frequencies unlike the higher frequencies.

5.3 Dynamic characteristics estimation

5.3.1 General overview

This section reports the results of implementation of the proposed estimation system in conjunction with ambient vibration measurements obtained by remote monitoring. For the

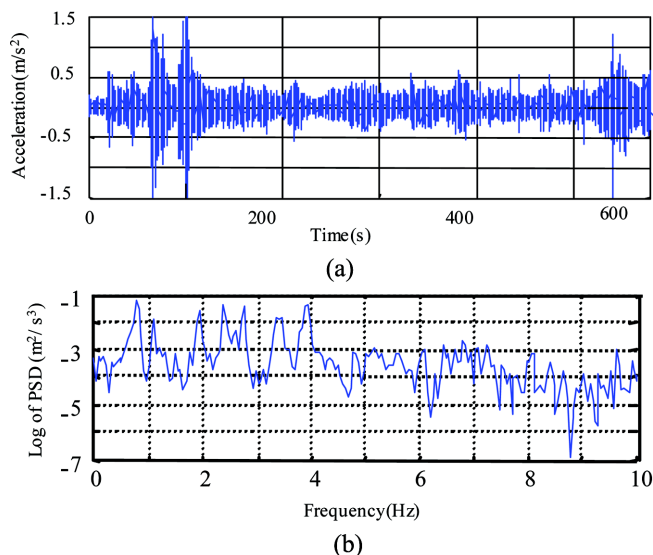


Fig. 7 Measured ambient vibration data (strong wind) (ch-2): (a) Measurement data, (b) Power spectrum density

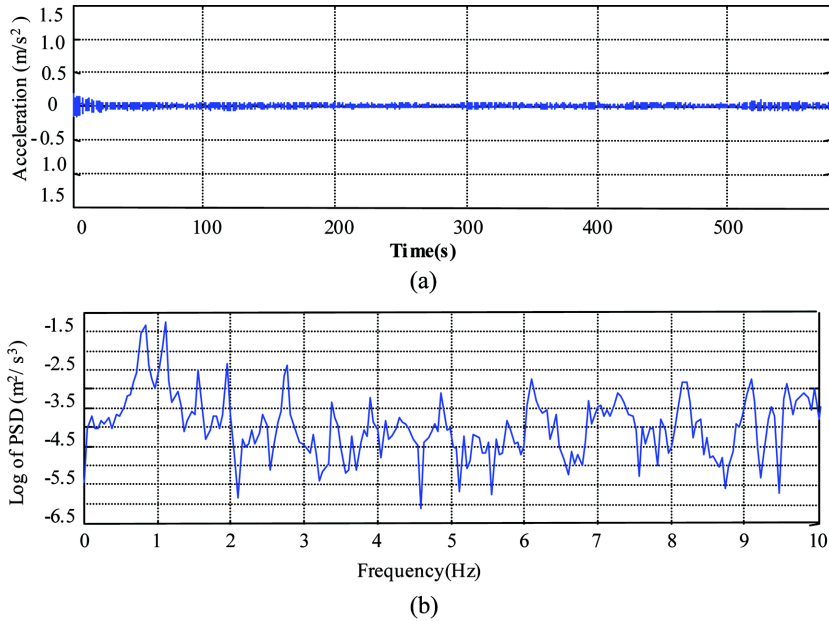


Fig. 8 Measured ambient vibration data (weak wind) (ch-2): (a) Measurement data, (b) Power spectrum density

calculation process, we considered the optimum size of N and k to be (5×200) and (5×40) respectively. One thousand two hundred (1200) data points were analyzed to estimate each set of dynamic characteristics and calculations were continued 25 times. The two different ambient vibration data samples were used to perform the estimation process by the SSR model I and SSR model II. In the following sections, graphical representations of the estimated dynamic parameters (natural frequencies, damping constants) are presented for the strong wind data, while a comparative presentation of the two methods is provided in tables. A general discussion of the estimated vibration modes is also presented.

5.3.2 SSR model I

a) Natural frequencies

Vibration natural frequencies are estimated by the SSR model I from the two types of ambient vibration data sample; the results obtained from the strong wind data are shown in Fig. 9(a). This demonstrates that natural frequencies for the first mode through seventh mode are estimated regularly. However, estimated natural frequencies above 4 Hz appear to be more scattered and cannot be separated clearly. On the other hand, with the weak wind data, natural frequencies above 4 Hz cannot be estimated regularly since weaker winds do not readily induce the higher modes. To illustrate this, Table 3 compares estimation accuracy for strong and weak wind data (up to seventh mode only). Estimated mean values for the two cases numerically very close. The coefficient of variation (CV) is similar up to the third mode, whereas it significantly higher for fourth, fifth, sixth, and seventh modes in the case of weak wind data. This signifies that better accuracy can be realized using strong wind data.

b) Damping constants

Following a similar process, the damping constants are evaluated. The results obtained using the

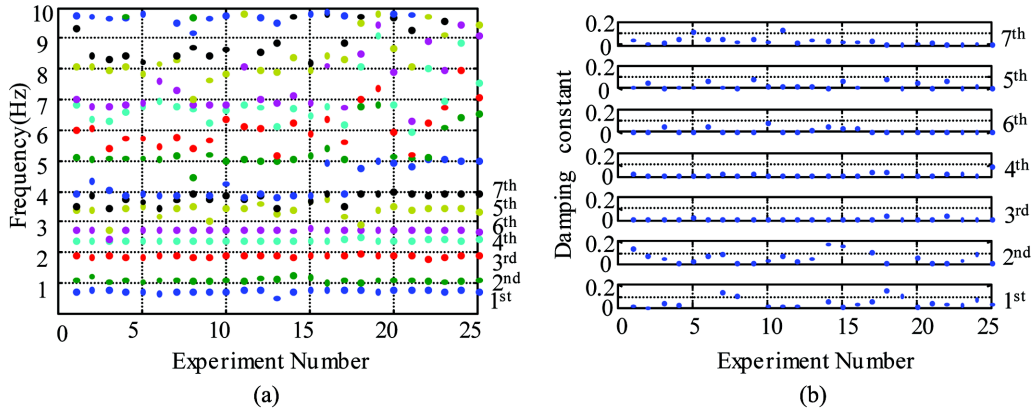


Fig. 9 Natural frequencies and damping constants estimated from strong wind induced vibration data (SSR model I): (a) Natural frequencies, (b) Damping constants

Table 3 Estimation accuracy evaluation; natural frequencies and damping constants were estimated using strong and weak wind induced ambient vibration measured from the real bridge; (SSR model I)

Mode number	Experiment condition	Estimated natural frequency (Hz)			Estimated damping constant		
		Mean	Standard deviation	Coefficient of variation (%)	Mean	Standard deviation	Coefficient of variation (%)
1 st	Strong wind	0.766	0.0562	7.34	0.1166	0.1931	165.64
	Weak wind	0.780	0.0498	6.38	0.0550	0.0974	176.96
2 nd	Strong wind	1.129	0.0594	5.26	0.0789	0.0993	125.86
	Weak wind	1.118	0.0118	1.06	0.0269	0.0338	125.80
3 rd	Strong wind	1.908	0.0315	1.65	0.0091	0.0113	124.83
	Weak wind	1.931	0.0265	1.37	0.0155	0.0228	147.49
4 th	Strong wind	2.426	0.0259	1.07	0.0141	0.0187	132.80
	Weak wind	2.485	0.0844	3.40	0.0272	0.0436	160.24
5 th	Strong wind	2.756	0.0607	2.20	0.0185	0.0232	125.14
	Weak wind	2.814	0.3009	10.69	0.0267	0.0344	128.93
6 th	Strong wind	3.402	0.2197	6.46	0.0366	0.0515	140.60
	Weak wind	3.367	0.4671	13.87	0.0345	0.0354	102.68
7 th	Strong wind	3.800	0.1768	4.65	0.0336	0.0332	98.94
	Weak wind	4.037	0.5585	13.83	0.0333	0.0389	116.60

strong wind data are presented in Fig. 9(b). As above, the accuracy of these estimates is compared in Table 3. The general conclusion to be drawn from this figure and table is that damping constants estimates are of considerably lower accuracy than the natural frequencies estimates; the CV values have a range 98-176%. This conclusion is consistent with the accepted understanding that estimated damping constants are usually not as accurate as frequencies. Comparatively higher values of damping constants for the first mode are estimated from the strong wind data. The possible causes might be due to the effect of external force (high wind force) on the systems damping properties. However, it is worth noting that the estimated mean damping constants are within a allowable range.

5.3.3 SSR model II

a) Natural frequencies

Vibration frequencies are estimated both for strong and weak wind data by the SSR model II. Results from the strong wind data are given in Fig. 10(a). This shows that frequencies from the first through seventh modes are estimated with a good level of consistency, whereas frequencies above 4 Hz cannot be clearly separated since the results deviate too much among estimates. A comparison of the results from strong wind and weak wind data samples is presented in Table 4. This reveals that the coefficient of variations for the strong wind sample is within 4.15% except in the case of the seventh mode; this value is lower than the result for the weak wind data. Again, strong wind

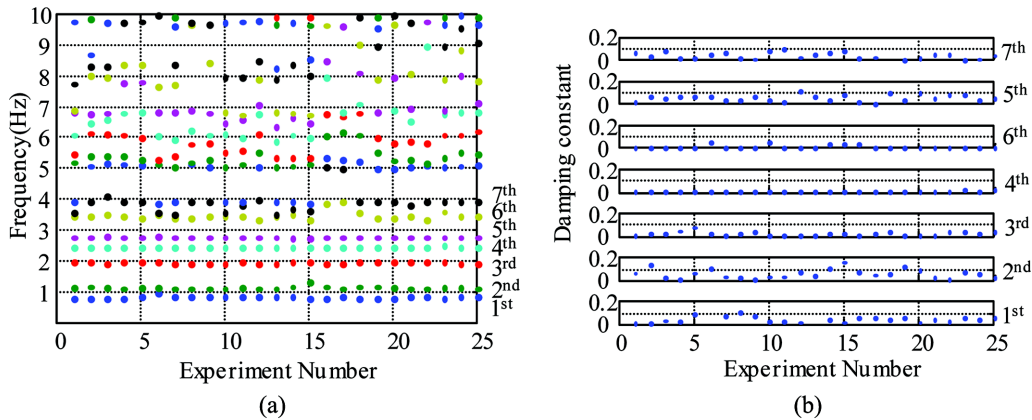


Fig. 10 Natural frequencies and damping constants estimated from strong wind induced vibration data (SSR model II): (a) Natural frequencies, (b) Damping constants

Table 4 Estimation accuracy evaluation; natural frequencies and damping constants were estimated using strong and weak wind induced ambient vibration measured from the real bridge; (SSR model II)

Mode number	Experiment condition	Estimated natural frequency (Hz)			Estimated damping constant		
		Mean	Standard deviation	Coefficient of variation (%)	Mean	Standard deviation	Coefficient of variation (%)
1 st	Strong wind	0.821	0.0269	3.28	0.0605	0.0546	90.21
	Weak wind	0.830	0.0345	4.16	0.0422	0.0553	131.29
2 nd	Strong wind	1.138	0.0405	3.56	0.0612	0.0427	69.71
	Weak wind	1.123	0.0156	1.39	0.0096	0.0087	90.61
3 rd	Strong wind	1.937	0.0141	0.73	0.0242	0.0167	68.79
	Weak wind	1.930	0.0128	0.66	0.0359	0.0481	134.06
4 th	Strong wind	2.427	0.0114	0.47	0.0065	0.0058	89.09
	Weak wind	2.284	0.1666	7.29	0.0591	0.0572	96.78
5 th	Strong wind	2.761	0.0092	0.33	0.0140	0.0161	115.12
	Weak wind	2.709	0.2675	9.87	0.0322	0.0293	90.93
6 th	Strong wind	3.481	0.1443	4.15	0.0576	0.0272	47.10
	Weak wind	3.471	0.6481	18.67	0.0492	0.0306	62.24
7 th	Strong wind	3.915	0.3777	9.65	0.0414	0.0338	81.75
	Weak wind	4.065	1.1074	27.24	0.0528	0.0322	61.01

induced data provides better estimation accuracy. Based on the results in Table 3 and Table 4, it is clear that the SSR model II offers better estimation accuracy as compared with the SSR model I.

b) Damping constants

Damping constants estimated from the strong wind data sample are presented in Fig. 10(b). There is some scatter in estimated damping constants for first and second modes, but there is more consistency than in the results obtained with the SSR model I. For comparison, estimated values are given in Table 4, which reveal that comparatively lower CV values are realized from the strong wind data.

5.3.4 Estimated vibration modes by SSR model I and SSR model II

Vibration modes are estimated separately by the SSR model I and SSR model II both strong wind and weak wind data samples. The estimated vibration modes obtained by the SSR model II from the strong wind data sample are presented in Fig. 11. These vibration modes plots are the averages of 25 estimates. The estimated first, second, third, and fifth mode vibrations are similar in shape to the modes of a typical arch-type steel truss bridge. The fourth mode is identical with the second mode and can be considered a torsional mode. Although the sixth and seventh modes are estimated, they are not symmetrical like a standard vibration modes. This is because the number of measurement points (five) is less than the mode number (seven).

5.3.5 Overall discussion on system identification process

In this paper a new method of system identification is proposed. Accordingly, the dynamic parameters of the existing bridge from first mode through seventh mode are estimated accurately. On the other hand, the estimation accuracy for the higher mode frequencies was not satisfactorily good. In the stochastic realization problem, the systems dynamic parameters are amalgamated with external forces and other noises. Besides, deterioration of sensors leading to errors and inaccuracy in measurement data and limited number of sensors produces limited data measurements (see, Takewaki and Nakamura 2005, Moustafa *et al.* 2010 for more details). Consequently, it is always very hard to extract systems real frequencies especially for the higher mode. In this regard, well distribution and increased number of sensors at the measurement system could provide better

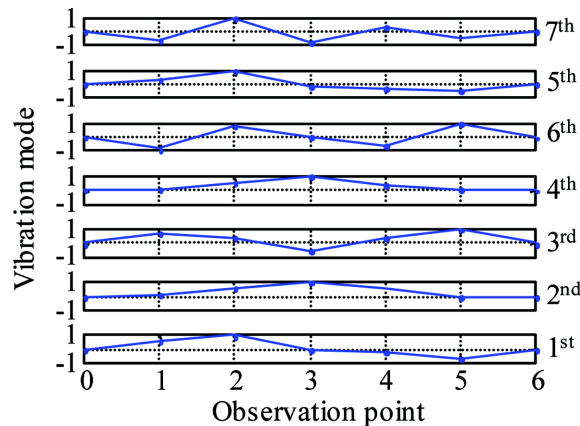


Fig. 11 Vibration modes estimated from strong wind induced vibration data (SSR model II)

accuracy. In addition, it is desirable to remove the noise from the measurements signals before carrying out the system identification to improve the estimation accuracy.

6. Conclusions

In this study, two subspace stochastic realization (SSR) theories (SSR model I and SSR model II) are investigated for estimating bridge dynamic characteristics (natural frequencies, damping constants, and vibration modes) from ambient vibration data. A remote monitoring system is prepared to collect the vibration data, which is operated by mobile communication. In this system, the sensors are instrumented on the bridge location and the vibration data is automatically collected by the server PC installed in the research laboratory and thus a dynamic characteristics estimation method is proposed. Two different sets of ambient vibration data samples were selected from the results of remote monitoring of the existing bridge: (a) data under strong wind condition collected during the summer storm and (b) data under weak wind condition corresponding to the normal wind condition around the bridge location. The results for the numerical simulation and remotely monitored data illustrate the usefulness of this method for estimating the dynamic characteristics of highway bridges using SSR theory.

(1) The numerical simulation demonstrated that subspace stochastic realization theories can effectively be used to estimate bridge dynamic characteristics (natural frequencies, damping constants, and vibration modes).

(2) The results obtained with ambient vibration data measured during strong and weak winds show distinct variations that prove the influence of data characteristics on estimation accuracy. In particular, better estimation accuracy is realized from high-amplitude (strong wind) ambient vibration data.

(3) Lower mode frequencies are effectively estimated from weak wind data, whereas estimation accuracy declines at higher modes because they are not readily induced by weak winds.

(4) The SSR model II gave better estimation accuracy than the SSR model I, both in the case of the simulation and the experimental data.

(5) Ambient vibration intensity and uniformity in amplitude should be taken into consideration in order to realize better accuracy in estimating bridge dynamic characteristics.

The dynamic characteristics of the bridge for the first seven modes are estimated accurately but the higher mode estimation is still a problem. This might be due to the existence of the measurement noise in the vibration data, influence of the excitation force, the wind dynamics and other environmental effects. These challenges may be overcome by denoising the measurement signals before carrying out the system identification. Furthermore, allowing sufficient number of sensors could help improving the estimation accuracy on higher mode frequencies. However, further investigations may be warranted to the improvement of estimation accuracy on the higher vibration modes. Besides, the quantification of the degree and the location of the bridge damage was not a target of this research. If such information is to be derived in future, the temperature variations and other changes in the surrounding environment during the monitoring period will need to be considered.

Acknowledgements

The Authors thank two anonymous reviewers for careful reading of the manuscript and for valuable comments made.

References

- Abdelghani, M., Verhaegen, M., Overschee, P.V. and Moor, B.D. (2001), "Comparison study of subspace identification methods applied to flexible structures", *Mech. Syst. Signal Pr.*, **12**(5), 679-692.
- Akaike, H. (1976), *Canonical correlation analysis of time series and the use of an information criterion, in system identification*, Advanced Case study (R. Mehra and D. Lainiotis, eds.), Academic, 27-96.
- Aoki, M. (1987), *State space modeling of time series*, Springer-Verlag, New York.
- Basseville, M., Benveniste, A., Goursat, M., Hermans, L., Mevel, L. and Van der Auweraer, H. (2001), "Output only subspace-based structural identification: from theory to industrial testing practice", *Trans. - ASME*, **123**, 668-676.
- Carden, E.P. and Brownjohn, M.W. (2008), "ARMA modeled time-series classification for structural health monitoring of civil structure", *Mech. Syst. Signal Pr.*, **22**, 295-314.
- Desai, U.B., Pal, D. and Kirkpatrick, R.D. (1985), "A realization approach to stochastic model reduction", *Int. J. Control*, **42**(4), 821-839.
- Gevers, A. (2006), "A personal view on the development of system identification a 30-year journey through an exciting field", *IEEE Contr. Syst. Mag.*, **26**(6) 93-105.
- Garibaldi, L., Girotcellini, E. and Piombo, B.A.D. (1998), "ARMAV techniques for traffic excited bridges", *J. Vib. Acoust. - ASME*, **120**, 713-718.
- Jimin, H. and Zhi-Fang, F. (2001), *Modal analysis*, Butterworth-Heinemann, Englewood cliffs, NJ.
- Juang, J.N. (1994), *Applied System Identification*, Prentice Hall PTR, Upper saddle River, NJ.
- Juang, J.N., Cooper, J.E. and Pappa, R.S. (1985), "An eigensystem realization algorithm for modal parameter identification and model reduction", *J. Guid. Control Dyn.*, **8**(5), 620-627.
- Katayama, T. (2005), *Subspace methods for system identification*, Springer Verlag, Berlin.
- Moustafa, A., Mahadevan, S., Daigle, M. and Biswas, G. (2010), "Structural and sensor damage identification using the bond graph approach", *Struct. Control Health Monit.*, **17**, 178-197.
- Nagayama, T., Abe, M., Fujino, Y., and Ikeda, K. (2005), "Structural identification of non proportionally damped system and its application to full-scale suspension bridge", *J. Struct. Eng.*, **131**(10), 1536-1545.
- Overschee, P.V. and Moor, B.D. (1996), *Subspace identification for linear systems*, Kluwer Academic Publishers, U.S.A.
- Papakos, V. and Fassois, S.D. (2003), "Multichannel identification of aircraft skeleton structures under unobservable excitation, A vector AR/ARMA framwok", *Mech. Syst. Signal Pr.*, **17**(6), 1271-1290.
- Peeters, B. and Roeck, G.D. (2001), "Stochastic system identification for operational modal analysis: a review", *J. Dyn. Syst. Measure. Control*, **123**, 659-667.
- Reyenders, E. and Roeck, G.D. (2008), "Reference-based combined deterministic-stochastic subspace identification for experimental and operational modal analysis", *Mech. Syst. Signal Pr.*, **22**, 617-637.
- Sohn, H., Farrar, C.R., Hemez, F.M., Shunk, D.D., Stinemat, D.W. and Nadler, B.R. (2003), "A review of structural health monitoring literature: 1996-2001", *Los Alamos National Lab.*, Report LA-13976-MS.
- Sirinngrong, D.M. and Fujino, Y. (2008), "System identification of suspension bridge from ambient vibration response", *Eng. Struct.*, **30**(2), 462-477.
- Takewaki, I. and Nakamura, M. (2005), "Stiffness-damping simultaneous identification user limited observation", *J. Eng. Mech. - ASCE*, **131**(10), 1027-1035.